17th Brazilian Congress of Thermal Sciences and Engineering
November 25th-28th, 2018, Águas de Lindóia, SP, Brazil

# SECOND LAW BASED CLOSED BRAYTON CYCLE REGENERATOR OPTIMIZATION

**Élvis Falcão de Araújo**
**Guilherme Borges Ribeiro**
**Lamartine Nogueira Frutuoso Guimarães**
Insitute for Advanced Studies - Trevo Coronel Aviador José Alberto Albano do Amarante, 1 - Putim
falcao@ieav.cta.br
gbribeiro@ieav.cta.br

***Abstract.*** *This work is a compilation of the research steps that were conducted in an optimization of a cross-flow heat exchanger, which is the regenerator of a Closed Brayton Cycle (CBC) to be used in space missions. Regenerative thermal cycles provide heat transfer between the hot and cold legs in the regenerator, which is responsible for increasing overall system efficiency. The downside is that the regenerator usually occupies the major part of system size because its effectivity depends on heat transfer area. In this context, a thermodynamics based regenerator optimization can be used in heat exchanger design. The second law of thermodynamics states that every process, from a thermal standpoint, produces entropy. In the Entropy Generation Minimization (EGM) method, the irreversibility generation rate, which is proportional to the Lost Available Work (LAW), is used as a Performance Evaluation Criteria (PEC) for system assessment and optimization. As fluid flows through both sides of the heat exchanger, entropy is produced by heat transfer and pressure drop, producing LAW. This study aims to find an optimum mass flow rate for the regenerator by evaluating a non-dimensional used to measure the entropy generation rate, the Entropy Generation Number ($N_s$), for multiples mass flow rate values, using 3D Computational Fluid Dynamics (CFD) as a support tool. The flow is solved in the heat exchanger's interior using the Finite Volume Method (VFM). Relevant fluid state properties are used for a second-law based optimization.*
***Keywords:*** *Closed Brayton Cycle, Regenerator, CFD, Entropy.*

## 1. INTRODUCTION

The concept of applying thermodynamic changes to a working fluid in order to draw power from a heat source is a common feature of multiple technologies released since the 18$^{th}$ century. The Closed Brayton Cycle (CBC) uses fluids above its critical temperature, also known as gases, to perform four thermodynamic processes in sequence: adiabatic compression, isobaric heating, adiabatic expansion and isobaric cooling. This concept is widely used in space nuclear reactors to convert fission thermal energy into power for electricity supply or propulsion. In space, system waste heat removal is done by radiation emitted from radiator panels. The CBC is preferred over other thermal cycles for high power space nuclear reactors because it offers the minimum ratio between system thermal efficiency and radiator area (Toro and Lior, 2017). Besides, the usage of gases avoids fluid phase changes that cause vibration.

The CBC thermal efficiency can be increased by using regenerators. These components provide heat transfer between fluids in the heat sink and heat source inlets, pre-heating the latter one and reducing the required thermal power from the heat source. In the proposed space power system, liquid metal heat pipes are responsible for the heat transport from the reactor to the CBC hot heat exchanger (CBC heat source). Water heat pipes perform the heat transport from the cold heat exchanger (CBC heat sink) to the radiators (Ribeiro *et al.*, 2015). Figure 1 includes a block diagram and a temperature-entropy plot of the proposed space power system.

This work aims to optimize the regenerator of a CBC applicable to a space reactor by using a non-dimensional second-law based performance evaluation criteria (PEC) called the Entropy Generation Number ($N_s$). The regenerator is a shell-and-tube, cross flow heat exchanger. The $N_s$ is evaluated for multiple mass flow rate values. The optimal mass flow is the one relative to the minimum $N_s$ value. This approach, proposed by Bejan (1982), is called the Entropy Generation Minimization (EGM) method.

The EGM analysis is supported by simulations using the commercial 3D Computational Fluid Dynamics (CFD) tool ANSYS – Fluent (ANSYS, 2016a), which applies the Finite Volume Method (FVM) to solve the turbulent flow inside the regenerator and obtain the temperature and pressure fields. The EGM is applied using data collected from the solver.

The regenerator CFD model draws inspiration from several past works in heat exchanger CFD simulation. Zhang *et al.* (2017) used CFD to simulate the flow in the intermediate heat exchanger of a sodium cooled fast reactor and Liu *et al.* (2017) used this tool to perform a multi-objective of a flat plate heat exchanger`s geometry using the ratio between the heat transfer coefficient and the friction factor as PEC. Multi-objective optimizations require the application of iterative routines, like the genetic algorithm used by Liu e*t al.* (2017).

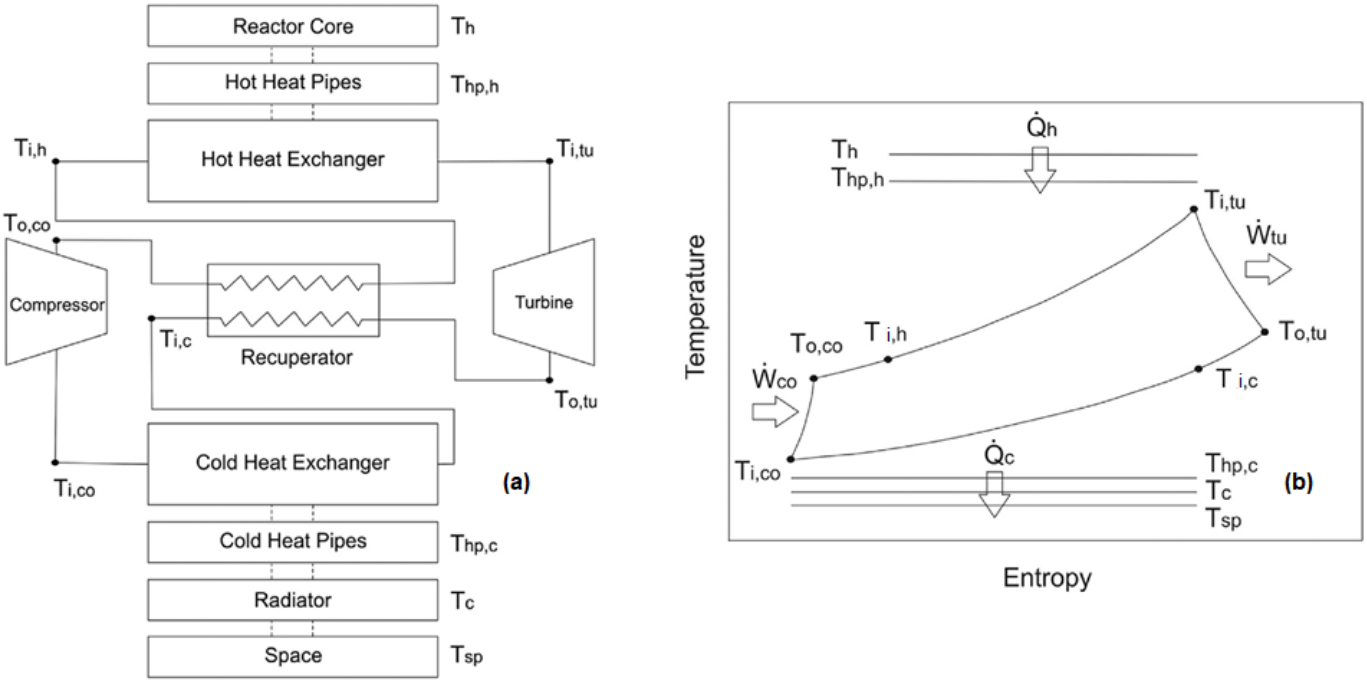


Figure 1. Proposed space power system (a) and Temperature-entropy diagram (b) (Ribeiro *et al.*, 2015).

The EGM optimization has been widely explored by researches of the thermal science field. Second law based analysis can provide data about the entropy generation behavior of a fluid flow or heat transfer process, allowing its study from a thermodynamic standpoint. The introduction of this approach by Bejan (1982) called the attention of the scientific community to the usage of second law analysis in CFD results interpretations.

Pussoli *et al.* (2012) made an analytical evaluation of the $N_s$ in peripheral finned-tube evaporators and generated multiple EGN curves by varying the flow Reynolds number and the evaporator geometry. Park and Kim (2016) used EGM to optimize a Submerged Combustion Vaporizer. Ye and Lee (2012) developed a numerical model based on EGM to design the refrigerant circuitry of a fin-and-tube condenser. Duarte *et al.* (2016) presented a microchannel heat sink design based on the entropy minimization criterion and a multi-objective optimization through several non-conventional algorithms.

Jafari *et al.* (2016) combined CFD and EGM to perform a multi-objective optimization of Diesel engines and compare its results with more conventional single-objective calculations. Kock and Herwig (2004) performed an in-depth analysis of turbulent flows and suggested how to calculate the entropy generation rates with the Reynolds Averaged Navier-Stokes (RANS) results. Ji *et al.* (2017) numerically investigated the entropy generation of fully turbulent convective heat transfer to nanofluids in a circular tube using the RANS model. Adesanya and Fakoya (2017) evaluated the entropy generation caused by slip flow and heat transfer through an infinite inclined channel filled with porous media. Zhou *et al.* (2017) developed a delayed detached-eddy simulation (DDES) based $k-\omega$ shear stress transport (SST) turbulence model using an entropy function to shield the flow boundary layer. This approach was compared with methods using other shielding functions and validated through a test case with large-scale vortex shedding.

This literature review shows the potential of applying the EGM to analyze CFD results, but there are obstacles to overcome in order to obtain more benefits from a second law based analysis. One of these barriers is the accuracy of the CFD results. The turbulence model used to solve the flow and obtain the temperature field strongly influences the entropy generation rates accuracy. The often-used RANS models may introduce considerable model errors (see Jin and Herwig, (2015)), while Large Eddy Simulation (LES) and Direct Numerical Solution (DNS) are more accurate, but their computational cost is too high for industrial problems. New models with increased accuracy and more acceptable computational costs should be developed in the future to allow more accurate entropy generation evaluations. In addition, the EGM principles were traditionally studied in thermodynamics, without further investigation of its applications in other areas. For example, studies on the use of EGM to interpret CFD results are relatively new. Further studies integrating second law based analysis to other scientific fields should be done in the future.

## 2. METHODOLOGY

### 2.1. Mathematical Model

The regenerator geometry is shown in fig. 2. It is a shell-and-tube, cross flow heat exchanger that has 4 rows of 3 tubes disposed around its center in a staggered disposition and with a 30º deviation from the radial orientation. The hot domain is contained in the shell side of the heat exchanger, representing the external flow around the tubes, while the cold domain is the internal flow contained in the tube side. For simplicity, the group of the tubes outer ends is considered the model cold outlet. The distance of 0.465 m between the inlets and the regenerator region prevents a uniform flow profile in the entrance of the heat exchanger area. Equation (1) evaluates the flow fully development path length for Newtonian fluids and laminar flows, where $D$ is hydraulic diameter, $\mu$ is dynamic viscosity and $Re$ is Reynolds number (Fox *et al.*, 2006). This equation is valid for laminar flows, while turbulent flows become fully developed with shorter path lengths.

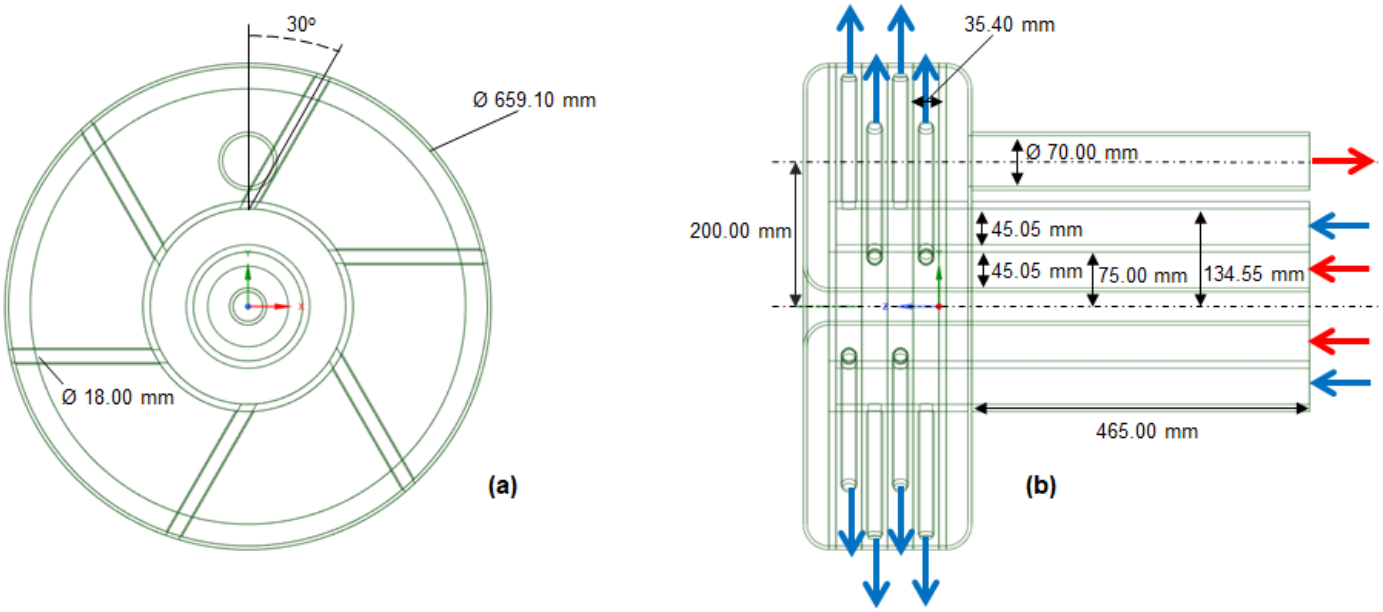


Figure 2. Regenerator geometry front view (a) and lateral view (b). The blue and red arrows indicate the model cold and hot ends, respectively.

$$\frac{L}{D} \cong \frac{0{,}06\,.\,(\rho V D)}{\mu} = 0{,}06\,.\,(Re) \tag{1}$$

The chosen materials for fluid and solid materials are respectively a 40 g/mol helium-xenon (He-Xe) mixture and Alloy 617 (10-15% Co, 20-24% Cr, 8-10% Mo, 0.8-1.5% Al, 0.05-0.15% C). The selection on the solid material is inspired by the Prometheus project, a nuclear electric propulsion (NEP) based space mission concept using a 200 kWe Brayton engine proposed by National Aeronautics and Space Administration (NASA) in 2003 (JPL, 2005). Alloy 617 was one of the materials under consideration for the Prometheus reactor loop piping (Ashcroft and Eshelman, 2007). It is a nickel-chromium-cobalt-molybdenum alloy with a combination of high-temperature strength and oxidation resistance. Wright *et al.* (2018) compiled several Alloy 617 creep and creep-rupture tests in the temperature range 800-1000 ºC performed by Idaho National Laboratory (INL) and Korea Atomic Energy Research Institute (KAERI). Larson-Miller analysis for 10-15% Co Alloy 617 at 1000 ºC revealed a creep-rupture time of approximately 20,9 years for 15% Co Alloy 617 under 7 Mpa. According to Ashcroft and Eshelman (2007), the Prometheus maximum temperature and pressure are respectively 1150 K and 2 Mpa, which validates the feasibility of using Alloy 617 as solid material for the CFD case, considering that space reactors are usually designed to have 10-15 years of operation life.

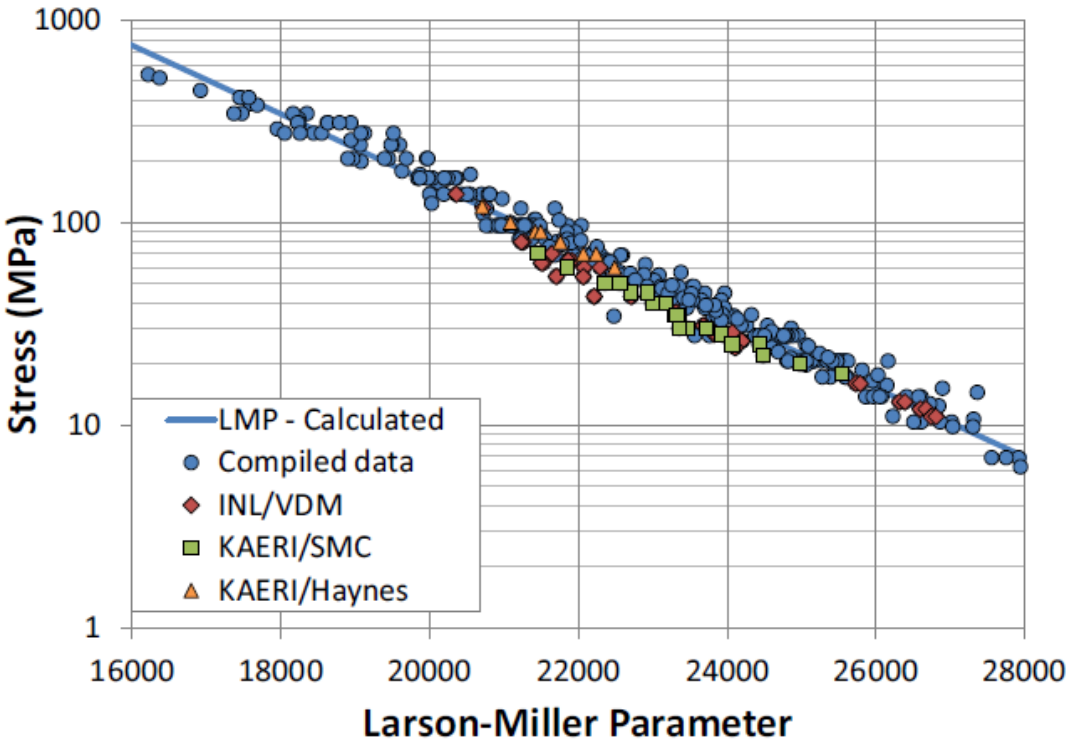


Figure 3. Larson-Miller plot for time to rupture of specimens tested in air with known chemistry (Wright *et al.*, 2018).

Figure 3 shows the Larson-Miller plot created by Wright *et al.* (2018) using rupture data from 348 creep tests for Alloy 617 with known chemical compositions that were tested in air. The Larson Miller Parameter (LMP) is related to the creep-rupture time by eqs. (2) and (3), where $C$ is the Larson Miller constant. This parameter was estimated as 16.73 by regression analysis for a linear fit.

$$LMP = a_0 + a_1 \log \sigma \tag{2}$$

$$\log t = \frac{a_0 + a_1 \log \sigma}{T} - C \tag{3}$$

The working fluid, a helium-xenon mixture, has been widely studied for reactor power plant design due to its good thermal-hydraulic properties. The decision of using a 40 g/mol (70% He) mixture is based on a solution-of-compromise between helium high heat capacity, which increases heat transfer rates, and xenon high molecular weight, which reduces turbomachine size demand. Relevant thermal materials of Alloy 617 (Metals, 2015), and He-Xe 40 g/mol (El-Genk; Tournier, 2007) are presented in tables 1 and 2. A linear interpolation is assumed for the properties that are variable with temperature.

Table 1. Alloy 617 properties.

| Property | Value |
|---|---|
| Thermal Conductivity (W/mK) | 18.82485 |
| Specific Heat Capacity (J/kgK) | 419 |
| Density (kg/m$^3$) | 8360 |

Table 2. He-Xe 40 g/mol properties.

| Property | Temperature (K) | Value |
|---|---|---|
| Thermal Conductivity (mW/mK) | 400 | 84.0896 |
| | 1200 | 183.4008 |
| Specific Heat Capacity (J/kgK) | 400 | 535.715 |
| | 1200 | 519.655 |
| Dynamic Viscosity (μPa.s) | 400 | 32.8571 |
| | 1200 | 74.2857 |

The model calculates fluid density by applying the state equation for incompressible ideal gases (see eq. (4), where $R$ is the universal gas constant, $M$ is gas molecular weight and $p_{op}$ is the operating pressure, which is 101325 Pa in this case). This assumption is valid for noble gases at low pressures and high temperatures, where the compressibility factor is approximately 1.

$$\rho = \frac{p_{op}}{\frac{R}{M}T} \tag{4}$$

The chosen temperature boundary conditions are 943 K in the hot inlet and 538 K in the cold inlet. These values were obtained in a prior design of the Prometheus reactor for a single 200 kWe Brayton unit (Ashcroft and Eshelman, 2007). Outlet boundary conditions are 101325 Pa pressure. The physical model also assumes a steady and incompressible flow.

### 2.2. The Finite Volume Method (VFM)

The FVM is a numerical tool that solves the flow inside of a given meshed domain through the integration and discretization the conservation equations in cell centers and the generation a linear system, which is solved by the Gauss Seidel method with under-relaxation factors. Equations (5), (6) and (7) dictate, respectively, the laws of continuity, momentum, and conservation of energy for incompressible flows (White, 1991). Turbulence is modelled with the realizable k-$\varepsilon$ model with standard wall function (ANSYS, 2016b), which includes two more equations that account for the transport of the turbulent kinetic energy (k) and the turbulent dissipation rate ($\varepsilon$) in the FVM approach.

$$\frac{\partial \rho}{\partial t} + \nabla \cdot (\rho \vec{V}) = 0 \tag{5}$$

$$\rho \left[ \frac{\partial \vec{V}}{\partial t} + (\vec{V} \cdot \nabla) \vec{V} \right] = -\nabla p + \nabla \cdot \bar{\bar{\tau}} + \rho \vec{F} \tag{6}$$

$$\rho \left[ \frac{\partial h}{\partial t} + \nabla \cdot (h \vec{V}) \right] = -\frac{\mathrm{D}p}{\mathrm{D}t} + \nabla \cdot (k \nabla T) + \phi \tag{7}$$

In these expressions, $\rho$ is density (kg/s), $V$ is velocity (m/s), $t$ is time (s), $p$ is pressure (Pa), $\bar{\bar{\tau}}$ is the stress tensor (Pa), $\vec{F}$ is the body forces resultant (N), $h$ is specific enthalpy (J/kg), $k$ is thermal conductivity (W/mK) and $\phi$ is the viscous dissipation function (Pa/s).

The solution uses a pressure based solver with a coupled scheme and 0.8 under relaxation factors for the turbulence equations. The used spatial discretization is first order upwind for momentum, turbulent kinetic energy, turbulent dissipation rate and energy, and linear for pressure. Residue tolerance is $10^{-3}$ for continuity, momentum and turbulence and $10^{-6}$ for energy.

### 2.3. The Entropy Generation Method (EGM)

The EGM method follows the principle that every thermodynamic system destroys available work by entropy generation. It assesses energy by its value in terms of convertibility from one form to another. The available work, also called exergy, is the fraction of the system energy that can be fully converted into useful power. It`s value is restricted by the two laws of thermodynamics. The Gouy-Stodola theorem makes a link between the exergy loss and the entropy generation in a control volume. It states that, in a thermodynamic system, the lost available work (LAW), also called anergy, is the product between the entropy generation rate and the environment temperature.

In the heat exchanger model developed in this work, exergy losses are assumed to occur only by entropy generation due to the flow pressure drop along the heat exchanger segments and the heat transfer between them. Therefore, considering a unidimensional case and neglecting other possible irreversibility sources, for high temperature flows, the entropy generation rate per unit length can be expressed by eq. (8) (Bejan, 1982), where $q'$ is heat flux per unit length (W/m), $T_w$ is wall temperature (K) and $\dot{m}$ is mass flow rate (kg/s). The first term in the right hand-side is associated with

generation of entropy due to heat transfer across a finite temperature difference and the second is relative to entropy generation due to fluid friction.

$$d\dot{S}_{gen} = \frac{q'(T_w - T)}{T^2} + \frac{\dot{m}}{\rho T}\left(-\frac{dp}{dx}\right) \tag{8}$$

Equation (9) expresses a heat exchanger entropy generation rate's integral form (Bejan, 1982), where the first two terms account for entropy generation associated with heat transfer and the last two terms represent entropy generated by pressure drop. In this expression, $c_p$ is specific heat capacity (J/kgK), $T_1$ the temperature relative to the heat exchanger hot side and $T_2$ to its cold side. This equation is valid for balanced heat exchangers, where the heat capacity rate is the same for the two sides.

The modelled regenerator is assumed as a balanced heat exchanger in this study. This assumption is based on the closed cycle regenerator definition, which states that the same fluid flows through the two sides with the same mass flow rate (specific heat variations with temperature are neglected). The entropy generation number, which is the parameter used as PEC, is expressed by eq. (10) (Bejan, 1982). As the specific heat is variable in this model, the mean value expressed by eq. (11) is used in the $N_s$ evaluation.

$$\dot{S}_{gen} = \dot{m}c_p \ln\left(\frac{T_1^{out}}{T_1^{in}}\right) + \dot{m}c_p \ln\left(\frac{T_2^{out}}{T_2^{in}}\right) - \dot{m}R \ln\left(\frac{p_1^{out}}{p_1^{in}}\right) - \dot{m}R \ln\left(\frac{p_2^{out}}{p_2^{in}}\right) \tag{9}$$

$$N_s = \frac{\dot{S}_{gen}}{\dot{m}c_p} \tag{10}$$

$$\bar{c}_p = \frac{c_p\left(T_1^{in}\right) + c_p\left(T_2^{in}\right)}{2} \tag{11}$$

## 3. RESULTS

### 3.1 Grid refinement sensitivity

A grid sensitivity study is performed by solving multiple CFD cases with different meshes and a fixed mass flow (0.1 kg/s) in order to choose a grid for the simulations in the parametrical study. This grid has to be efficient and to give an accurate solution, which means that the results should not vary considerably with the use of more refined meshes, eliminating the need for further grid refinement that would impact on computational cost increase without a substantial accuracy gain. The grids have the same mesh generation algorithm. In this study, the grid refinement is measured by *l*, the element size inside the tubes. Table 3 correlates the grid number of elements with *l* for various meshes.

Table 3. Number of elements in function of tube interior element size.

| *l* (mm) | Number of elements (-) |
|---|---|
| 5 | 984510 |
| 4 | 1254307 |
| 3 | 1747957 |
| 2 | 3521590 |
| 1.5 | 6317637 |
| 1 | 15821218 |
| 0.5 | 80746464 |

Temperature values of 26 equidistant points along the center of a selected tube are collected in the same positions for all tested grids. Figure 4 shows the temperatures curves obtained. Like expected, the result sensitivity with mesh refinement is reduced as the tube interior element size decreases.

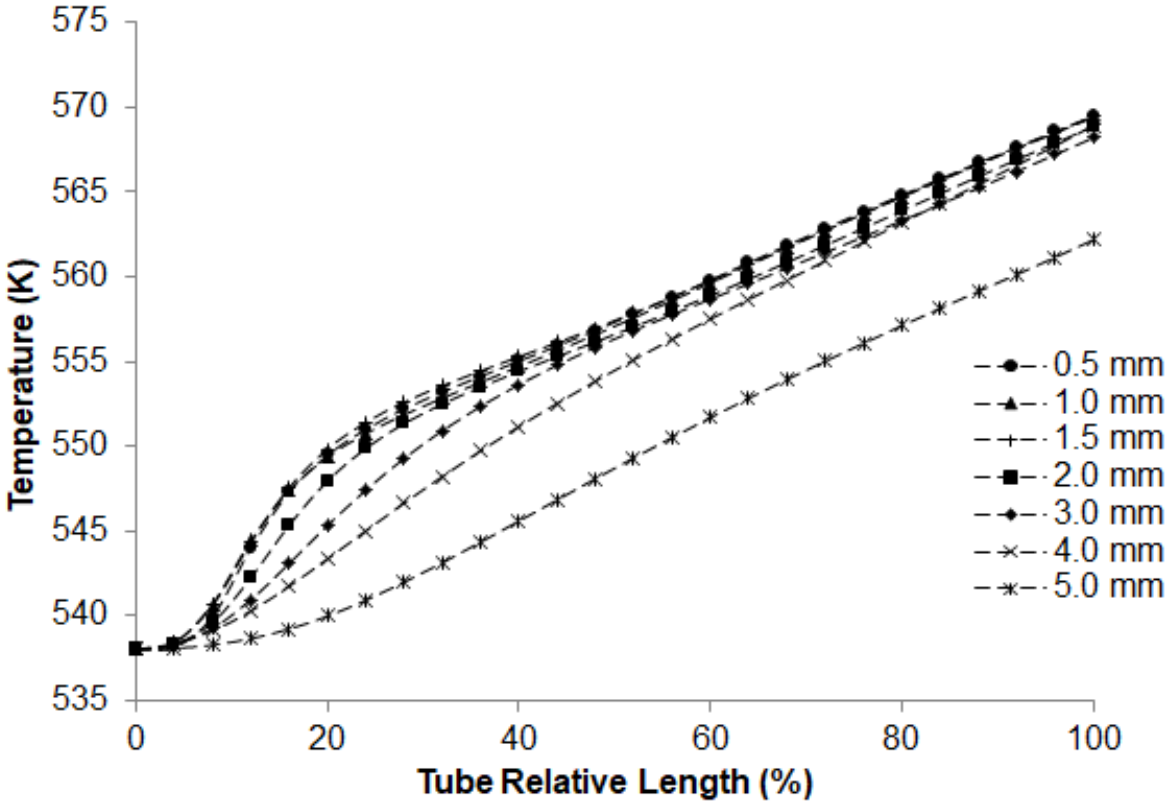


Figure 4. Grid refinement sensitivity study.

The figure-of-merit expressed by eq. (12) is defined as the error between the mesh results of two consecutive grids in the refinement scale. In this expression, $T_{g1}$ refers to the temperature values obtained with the coarse grid, while $T_{g2}$ to the ones obtained with the fine grid. Using this metric, the chosen mesh is the coarser one in a group of three consecutive grids that have two errors $e_1$ and $e_2$ such that $e_1$, $e_2 < 0.050$.

$$e = \max \left. \frac{T_{g1}^{i} - T_{g2}^{i}}{T_{g2}^{25} - T_{g2}^{0}} \right|_{i=0}^{25} \tag{12}$$

Table 4 shows the errors obtained by applying eq. (12) to the temperature values displayed in fig. 4. According to the mesh selection criteria described previously, the grid with $l$ = 1.5 mm is the most likely to provide accurate solutions without excessive computational cost, therefore being the one used for the simulations in the second law based parametrical study.

Table 4. Grid refinement sensitivity study results.

| $l$ (mm) | Error (-) |
|---|---|
| 5 | 0.218 |
| 4 | 0.894 |
| 3 | 0.850 |
| 2 | 0.717 |
| 1.5 | 0.023 |
| 1 | 0.024 |

### 3.2 Entropy generation number ($N_s$)

The results for the entropy generation number curves are obtained through the application of eqs. (9) and (10) to the end temperatures and pressures of the domain after the flow solution by the FVM. This procedure is done 10 times, using a variable mass flow rate whose value vary from 0.02 kg/s to 0.11 kg/s.

Figure 5 shows the influence of the mass flow rate on the entropy generation number associated to pressure drop. Its value increases from 0.005 x $10^{-1}$ to 0.012 as the mass flow rate rises. Higher flow velocities induce increases in the major (related to fluid friction) and minor (produced by bends, fittings, sudden area changes, etc) head losses, which lead to increments in the flow pressure drop. Consequently, the irreversibility associated to this phenomena increases with mass flow rate as well.

Figure 6 shows the influence of the mass flow rate on the entropy generation number produced by heat transfer. Its value decreases from 0.050 to 0.035 as the mass flow rate rises. The regenerator effectiveness decreases with mass flow rate, which reduces the fluid temperature gradient along its flow inside the regenerator and consequently, the irreversibility related to heat exchange.

It can be seen that, in the majority of the mass flow rate regimes, the heat transfer $N_s$ values are significantly higher than the pressure drop $N_s$, presenting a lower difference only in higher mass flow rates. This is expected of a heat exchanger, where there is a need to augment heat transfer and minimize pressure drop. In industrial applications, heat exchanger engineering must provide minimum $N_s$ without reducing heat exchanger effectiveness. This can be done by increasing the exchanger available area or changing the working fluid.

Figure 7 shows the total entropy generation number dependence on the mass flow rate. The total $N_s$ produced by the flow field obtained by each CFD simulation is evaluated by summing the two portions (pressure drop and heat transfer) previously presented. The obtained profile agrees with the EGM theory proposed by Bejan (1982). The design point with minimum $N_s$ presented below is the one that has minimum LAW embedded within it, being the optimum configuration from a thermodynamic standpoint.

The minimum $N_s$ is 0.043, obtained at $\dot{m}$ = 0.07 kg/s. This corresponds to Reynolds numbers *Re* = 5562.69 in the cold inlet and *Re* = 7616.05 in the hot inlet, which confirms the hypothesis of a turbulent internal flow and the necessity of using the k-$\varepsilon$ viscous model. In these conditions, the entropy generation rate for $\bar{c}_p$ = 528.88 J/kgK is 1.62 W/K and the lost available work for an environment temperature of 300 K is 486 W.

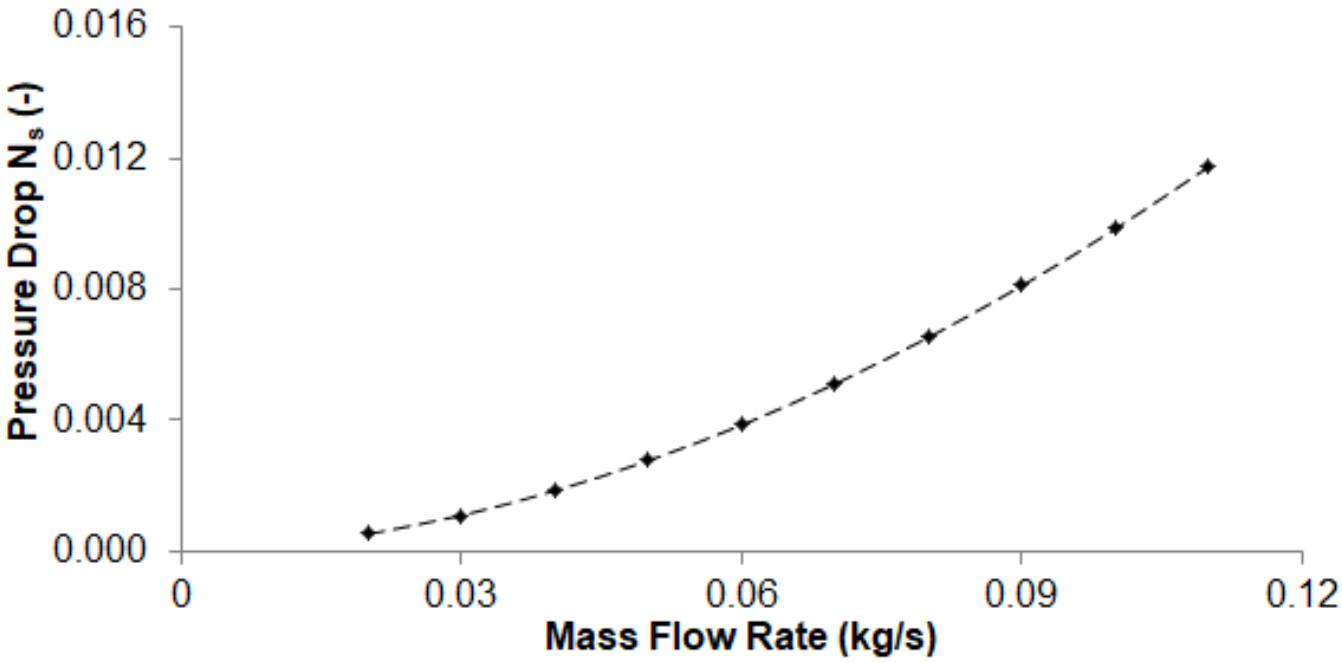


Figure 5. Pressure drop entropy generation number profile.

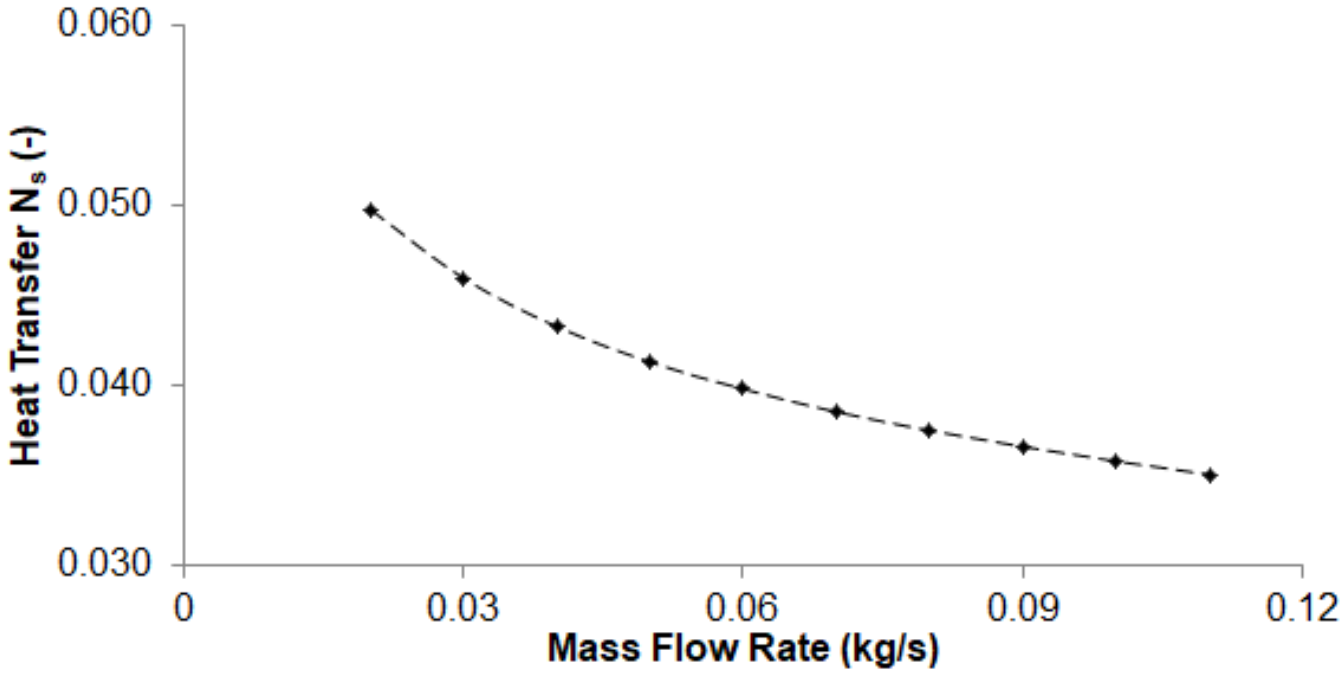


Figure 6. Heat transfer entropy generation number profile.

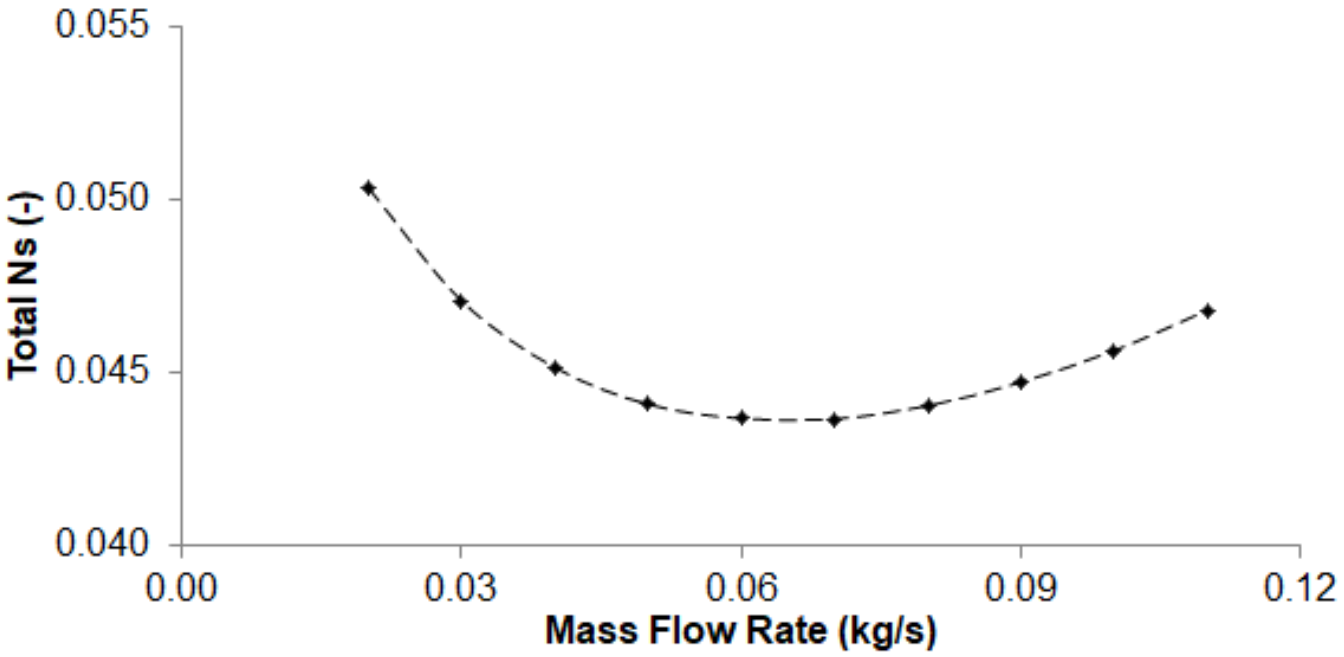


Figure 7. Total entropy generation number profile

## 4. CONCLUSIONS

The numerical results for pressure drop and heat transfer entropy generation numbers presented in figs. 5 and 6 are coherent with the theoretical expectations, although the entropy generation evaluation accuracy is limited by the RANS turbulence model, which introduces several errors. Heat transfer between the two sides of the heat exchanger is enhanced in lower velocities, while pressure drop values raise with velocity increase, so the $N_s$ is expected to follow these tendencies as the mass flow rate vary. Besides, the irreversibility related to heat transfer is considerably higher than the one associated to pressure drop in the optimum regenerator design point.

The minimum total $N_s$ (displayed in fig. 7) and optimum Reynolds numbers obtained for this regenerator configuration are moderate, showing that the heat exchanger can be optimized by changing regenerator geometry. Some geometric changes envisioned are increasing the number of tubes in the azimuthal and longitudinal directions, with the disadvantage of increasing the regenerator mass and size, which is not desirable for space applications. A trade-off study between mass and efficiency is the best way to find the optimum configuration.

## 5. REFERENCES

Adesanya, S.O., Fakoya, M. B., 2017, "Second Law Analysis for Couple Stress Fluid Flow through a porous medium with constant heat flux", Vol. 19, 498.

ANSYS, 2016a. "Module A: Introduction to ANSYS Inc., Introduction to ANSYS Fluent", Ansys Inc., 12 April. 2016, <https://www.ansys.com>.

ANSYS, 2016b. "Module 07: Turbulence, Introduction to ANSYS Fluent", Ansys Inc., 12 April. 2016, <https://www.ansys.com>.

Ashcroft, J. and Eshelman, C., 2007, "Summary of NR Program Prometheus Efforts". In *Proceedings of the Space Technology and Applications International Forum – STAIF 2007*. College Park, Maryland, USA.

Bejan, A., 1982, *Entropy Generation through heat and fluid flow*. John Wylen & Sons, New York.

Duarte, J. M. C., Perez, A.G. and Contreras, I.M.A., 2016, "Designing a microchannel heat sink with colloidal coolants through the entropy generation minimization criterion and global optimization algorithms", Applied Thermal Engineering, Vol. 100, pp. 1052-1062.

El-Genk, M.S. and Tournier, J.M., 2008, "Noble gas binary mixtures for gas-cooled reactor power plants", *Nuclear Engineering and Design*, Vol. 238, pp. 1353-1372.

Fox, R.W, Mcdonald, A.T., Pritchard, P.J., 2006, *Introduction to Fluid Mechanics*. John Wyley & Sons, USA.

HTM, 2015. "Inconel 617 Technical Data" High Temperatuyre Metals. 28 Mar. 2018 < http://www.hightempmetals.com/techdata/hitempInconel617data.php>

Jafari, M. *et al.*, 2016, "Inclusion of entropy generation minimization in multi-objective CFD optimization of diesel engines", Energy, Vol. 114, pp. 526-541.

Jet Propulsion Laboratory, 2005, *Prometheus Project: Final Report*, National Aeronautics and Space Administration (NASA), Pasadena, California, USA, NASA/982-R120461, 215p.

Ji, Y., Zhang, H.C., Yang, X. and Shi, L., 2017, "Entropy Generation Analysis and Performance Evaluation of Turbulent Forced Convective Heat Transfer to Nanofluids", Entropy, Vol. 19, 108.

Jin, Y. and Herwig, H., 2015, Turbulent flow in rough wall channels: Validation of RANS models. Comput. Fluids , Vol. 122, 34–46.

Kock, F. and Herwig, H., 2004, "Local entropy production in turbulent shear flows: A high-Reynolds number model with wall functions", International Journal of Heat and Mass Transfer, Vol. 47, pp. 2205-2215.

Liu, C., Bu, W. and Xu, D., 2017, "Multi-objective shape optimization of a plate-fin heat exchanger using CFD and multi-objective genetic algorithm", International Journal of Heat and Mass Transfer, Vol. 111, pp. 65-82.

Pussoli, B.F., Barbosa Jr., J.R., da Silva, L.W. and Kaviany, M., 2012, "Optimization of peripheral finned-tube evaporators using entropy generation analysis minimization", *International Journal of Heat and Mass Transfer*, Vol. 55, pp. 7838-7846.

Park. Y.C. and Kim, J., 2016, "Submerged combustion vaporizer optimization using Entropy Minimization Method", Vol. 103, pp. 1071-1076.

Ribeiro, G.B., Braz Filho, F.A., Guimarães, L.N.F., 2015, "Thermodynamic analysis and optimization of a Closed Regenerative Brayton Cycle for nuclear space power systems", *Applied Thermal Engineering*, Vol. 90, pp. 250-257.

Toro, C. and Lior, N., 2017, "Analysis and Comparison of Solar-Heat driven Stirling, Brayton and Rankine cycles for space power generation", *Energy*, Vol. 120, pp. 549-564 .

White, F.W., 1991, *Viscous Fluid Flow*. McGraw-Hill, 2nd edition.

Wright, J.K., Lillo, T.M., Wright, J.R., Kim, W.G., Sah, I.J., Kim, E.S., Park, J.Y., Kim, M.H., "Creep and creep-rupture of Alloy 617", *Nuclear Engineering and Design*, Vol. 329, pp. 142-146.

Yee, H.Y. and Lee, K.S., 2012, "Refrigerant circuitry design of fin-and-tube condenser based on entropy generation minimization", *International Journal of Refrigeration*, Vol. 35, pp. 1430-1438.

Zhang, X., Tseng, P. and Saeed, M., 2017, "A CFD-based simulation of fluid flow and heat transfer in the Intermediat e Heat Exchanger of sodium-cooled fast reactor", *Annals of Nuclear Energy*, Vol. 109, pp. 529-537.

Zhou, L., Zhao, R. and Shi, X. P., 2017, "An Entropy-Assisted Shielding Function in DDES Formulation for the SST T urbulence Model", Entropy, Vol. 19, 93.